Effects of spin-exchange collisions in a high-density alkali-metal vapor in low magnetic fields

I. M. Savukov and M. V. Romalis
Department of Physics, Princeton University, Princeton, New Jersey 08544, USA
(Received 24 August 2004; published 10 February 2005)

Spin-exchange collisions often play a dominant role in the broadening of Zeeman resonances in an alkali-metal vapor. Contrary to intuitive expectations, at high alkali-metal densities this broadening can be completely eliminated by operating in a low magnetic field, allowing construction of ultrasensitive atomic magnetometers. We describe a detailed study of the Zeeman resonance frequencies and linewidths as a function of the magnetic field, alkali-metal density, and the degree of spin polarization of the atoms. Due to the nonlinear nature of the density matrix equations describing the spin-exchange collisions both the gyromagnetic ratio and the linewidth change as a function of the polarization. The results of experimental measurements are in excellent agreement with analytical and numerical solutions of the density matrix equations.

DOI: 10.1103/PhysRevA.71.023405 PACS number(s): 33.35.+r, 07.55.Ge, 32.80.Bx

I. INTRODUCTION

It has been known for a long time that spin-exchange (SE) collisions between alkali-metal atoms broaden magnetic resonance lines [1]. This broadening, which is proportional to the density of the alkali-metal vapor, was used, for example, to obtain the SE cross sections [2–4]. In 1973 Happer and Tang [5] discovered experimentally that magnetic resonances can be *narrowed* by increasing the density of alkali atoms in a low magnetic field. A few years later, Happer and Tam [6] carried out a detailed theoretical investigation of this effect based on the density matrix formalism developed in [7–10] and were able to derive an analytical solution in the limit of low spin polarization. In addition, the statistical analysis of the effects of spin exchange was given, showing its similarity to such effects as motional narrowing of NMR lines in liquids.

SE effects for arbitrary polarization in the limit of zero magnetic field were first studied in [11]. It was shown that spin-exchange broadening can be completely eliminated in this regime. The combination of high alkali-metal density, high spin polarization, and narrow magnetic resonance is particularly beneficial for precision measurements. Atomic magnetometers based on this technique have exceeded the sensitivity of low-temperature SQUID magnetometers [12]. It was also shown theoretically [11] that in this regime the frequency of the Zeeman resonance depends on the spin polarization due to the nonlinear nature of the density matrix evolution caused by the SE collisions.

SE effects in the case of arbitrary SE rate, magnetic field, and polarization have not been systematically investigated. Therefore, in this paper we study experimentally and theoretically SE effects in this general case. We compare our experimental measurements of the gyromagnetic ratios and widths of the magnetic resonances for a relatively large range of SE rates, magnetic fields, and polarization with analytical results derived in [6,11] as well as with full numerical solutions of the density matrix equations. Detailed understanding of the effects of SE collisions is important for operation of high sensitivity alkali-metal magnetometers. For example, the variation of the gyromagnetic ratio with the polarization can cause additional broadening due to polarization inhomogeneities unless the magnetometer is operated near zero field. The dependence of the Zeeman resonance width on the magnetic field determines the range of magnetic fields where the magnetometer is most sensitive.

Spin-exchange effects can also be used to determine the properties of the alkali-metal vapor in various optical pumping experiments. For example, measurements of SE broadening at low magnetic field provide a simple way to determine the density of the alkali-metal vapor using a known cross section of SE collisions. The average spin polarization of the vapor can also be determined from measurements of the gyromagnetic ratio in low magnetic field. We found these techniques to be very convenient.

In addition to the SE effects in low magnetic fields, two other counterintuitive effects related to SE collisions have been observed. In 1981, Bhaskar *et al.* [13] discovered "light narrowing" of magnetic resonances caused by an increase of laser intensity in the presence of a strong RF excitation field. This phenomenon can be explained by the Bloch equations as a reduction of the RF power broadening [14].

Another type of "light narrowing" of magnetic resonances was observed by Appelt *et al.* [15] in a high magnetic field. This effect is caused by a reduction of SE broadening due to optical pumping of most atoms into a stretched state unaffected by spin-exchange collisions. A similar narrowing effect for microwave transitions has also been recently observed [16]. These effects can be analyzed quantitatively based on theoretical analysis presented in Ref. [17]. Both "light narrowing" effects have also been observed in our measurements and will be briefly discussed.

II. THEORY

A. Simple model of spin exchange

The basic phenomenon of SE broadening of magnetic resonance lines and its dependence on the magnetic field and the SE rate can be understood from simple qualitative arguments. The density matrix of the alkali atoms can be written as a sum of contributions from the two ground-state hyperfine components $F=I+1/2\equiv a$ and $F=I-1/2\equiv b$, $\rho=\rho_a+\rho_b$. Under typical conditions in atomic magnetometers the atoms

 ©2005 The American Physical Society

spend a negligible amount of time in the excited state and the coherences between the two hyperfine states can be neglected in the absence of microwave fields. We can introduce the total angular momenta in each of the two hyperfine states $\mathbf{F}_a = \mathrm{Tr}[\mathbf{F}\rho_a]$ and $\mathbf{F}_b = \mathrm{Tr}[\mathbf{F}\rho_b]$. In a magnetic field the angular momenta in the two hyperfine states precess in opposite direction with a frequency ω_0,

$$\frac{d\mathbf{F}_a}{dt} = -\omega_0[\mathbf{B}\times\mathbf{F}_a], \tag{1}$$

$$\frac{d\mathbf{F}_b}{dt} = +\omega_0[\mathbf{B}\times\mathbf{F}_b]. \tag{2}$$

The spin precession frequency ω_0 is reduced compared to that of a free electron due to the hyperfine interaction by the ratio of the reduced matrix elements of $\hat{S}$ and $\hat{F}$ operators:

$$\frac{\omega_0}{g_S\mu_B B/\hbar} = \frac{\langle F_{a,b}\|S\|F_{a,b}\rangle}{\langle F_{a,b}\|F\|F_{a,b}\rangle} = \pm\frac{1}{2I+1}. \tag{3}$$

The SE collisions conserve the total angular momentum,

$$\mathbf{F}_a + \mathbf{F}_b = \mathbf{F}'_a + \mathbf{F}'_b, \tag{4}$$

but can transfer the atoms between the hyperfine states and tend to align the polarization in the two states. The balance between the magnetic field torque and the SE relaxation determines the angle between $\mathbf{F}_a$ and $\mathbf{F}_b$. Consider precession around B_y magnetic field with $\mathbf{F}_a$ and $\mathbf{F}_b$ initially parallel to the z axis. If the time between SE collisions T_{SE} is much smaller than the precession frequency, then the angle between $\mathbf{F}_a$ and $\mathbf{F}_b$ is small and one can write the following equation using the conservation of the angular moment for the x-component of $\mathbf{F}$,

$$-\omega_0 dt F_{az} + \omega_0 dt F_{bz} = \omega dt(F_{az} + F_{bz}). \tag{5}$$

Solving for ω we obtain the precession frequency of the total vector $\mathbf{F}_a + \mathbf{F}_b$,

$$\omega = \omega_0\frac{F_{az} - F_{bz}}{F_{az} + F_{bz}}. \tag{6}$$

In the regime of fast spin-exchange collisions the longitudinal steady-state solution usually satisfies the spin-temperature distribution [9,17]

$$\rho \propto e^{\beta F_z}, \tag{7}$$

where β is the spin-temperature parameter,

$$\beta = \ln\left(\frac{1+P}{1-P}\right). \tag{8}$$

Using the spin temperature distribution we can rewrite Eq. (6) in terms of the parameter β. For $I=3/2$

$$\omega = \omega_0\frac{2\cosh\beta}{1+2\cosh\beta}, \tag{9}$$

in agreement with [11] or in terms of the polarization $P = \tanh(\beta/2)$,

$$\gamma \equiv \omega/\omega_0 = 2 - \frac{4}{3+P^2}. \tag{10}$$

Here we defined a dimensionless gyromagnetic ratio γ. For $I=5/2, I=7/2$, by substituting the spin-temperature distribution into Eq. (6) we obtain

$$\gamma(I=5/2) = 3 - \frac{48(1+P^2)}{19+26P^2+3P^4}, \tag{11}$$

$$\gamma(I=7/2) = \frac{4(1+7P^2+7P^4+P^6)}{11+35P^2+17P^4+P^6}. \tag{12}$$

The zero polarization limit of these expressions gives $\gamma(I) = 3(2I+1)/((2I+1)^2+2)$ in agreement with the result obtained in Ref. [6].

When the SE rate decreases and approaches the precession frequency, the angle between the angular momenta in the two hyperfine states increases. We can derive an approximate relationship for the transverse spin relaxation if we assume that only the common component of $\mathbf{F}_a$ and $\mathbf{F}_b$ survives the spin-exchange collisions. Then

$$T_2^{-1} \simeq \frac{1-\cos(\omega_0 T_{SE})}{T_{SE}} \simeq \omega_0^2 T_{SE}, \tag{13}$$

where T_{SE} is time between spin-exchange collisions. Thus the transverse relaxation rate due to SE collisions goes to zero as B^2 in low magnetic fields. These results are in agreement with more elaborate calculations using the full density matrix equations.

B. Density matrix equations

Our calculations are based on the density matrix equation derived in Ref. [17]:

$$\frac{d\rho}{dt} = a_{hf}\frac{[\mathbf{I}\cdot\mathbf{S},\rho]}{i\hbar} + \mu_B g_S\frac{[\mathbf{B}\cdot\mathbf{S},\rho]}{i\hbar} + \frac{\varphi(1+4\langle\mathbf{S}\rangle\cdot\mathbf{S}) - \rho}{T_{SE}} + \frac{\varphi-\rho}{T_{SD}} + R[\varphi(1+2\mathbf{s}\cdot\mathbf{S}) - \rho] + D\nabla^2\rho, \tag{14}$$

where $\varphi = \rho/4 + \mathbf{S}\cdot\rho\mathbf{S}$ is the purely nuclear part of the density matrix ρ, a_{hf} is the hyperfine coupling constant, $g_S \simeq 2$ is the electron's g factor, $\mu_B = 9.27\times10^{-21}$ erg/G is the Bohr's magneton, and $\langle\mathbf{S}\rangle = \mathrm{Tr}[\rho\mathbf{S}]$. T_{SD} is the spin-destruction relaxation time, R is the optical pumping rate, D is the diffusion constant, and $\mathbf{s}$ is the optical pumping vector which defines the direction and the degree of circular polarization of the pumping light. The first two terms on the right-hand side of Eq. (14) describe the hyperfine and magnetic interactions. The SE collisions are described by the third term with the SE rate given by

$$A_{SE} = 1/T_{SE} = n\bar{v}\sigma_{SE}. \tag{15}$$

Here n is the density of alkali-metal atoms, $\bar{v}$ is their average relative velocity, and σ_{SE} is the spin-exchange cross section. The fourth term describes spin relaxation at a rate $A_{SD} = T_{SD}^{-1}$ due to binary collisions with a buffer gas that relax the

electron spin while preserving the nuclear part of the polarization. The effects of van der Waals molecules are negligible in the presence of high buffer gas pressure. The fifth term describes optical pumping at a rate R in the regime where the hyperfine structure of the alkali atoms is not resolved optically due to large pressure broadening. One also assumes that the excited state population is quickly quenched by collisions with N_2 buffer gas. The last term describes the diffusion of the alkali atoms. In the absence of a surface coating both the electron and nuclear polarizations at the walls of the cell are relaxed to zero. The equilibrium spin polarization of the atoms is determined by the optical pumping, spin relaxation, and diffusion to the walls, it is not affected by the SE process. If the diffusion-limited wall relaxation is slow compared to other processes, then the distribution of atoms among different Zeeman and hyperfine sublevels is given by the spin-temperature distribution (7) [17]. In the experiment we apply a constant B_z field parallel to the pump laser and a small oscillating B_y field to excite the Zeeman resonance. The spin-temperature distribution and the z projection of the polarization, $P_z=\tanh(\beta/2)$ are not affected by a sufficiently small B_y field. SE only causes relaxation of the transverse components of the polarization.

III. NUMERICAL SIMULATIONS

Numerical simulation is the most straightforward approach to investigate the range of input parameters for which a simple analytical solution cannot be found. The density matrix can be expanded in a complete basis of coupled hyperfine states

$$\rho=\sum_{ij}\rho_{ij}|i\rangle\langle j| \tag{16}$$

and Eq. (14) can be solved for example using Euler-Cauchy or classical Runge-Kutta method. Any operator in Eq. (14) can be represented by a $2(2I+1)\times 2(2I+1)$ matrix, with the rules for the product of operators replaced with a normal rule of matrix multiplication. Because the operators depend on nuclear and electron spins we can express them in terms of matrix elements of **S** and **F**, which can be easily found in the spherical basis.

We are interested mostly in the case when the hyperfine term is much larger than the magnetic and SE terms. A large hyperfine constant requires a tiny step in integration, which slows down computation considerably. However, in the limit of a large hyperfine constant the problem can be simplified because the density matrix elements off-diagonal in F are oscillating with the hyperfine frequency and average to zero. By using the projection operator

$$\Pi\left\{\begin{bmatrix}\rho_a & * \\ * & \rho_b\end{bmatrix}\right\}=\begin{bmatrix}\rho_a & 0 \\ 0 & \rho_b\end{bmatrix} \tag{17}$$

that sets off-diagonal in F matrix elements to zero after the action of spin-exchange and other terms, we can exclude the hyperfine term. We checked that the solutions are the same when hyperfine term was included and when the projection operator was used.

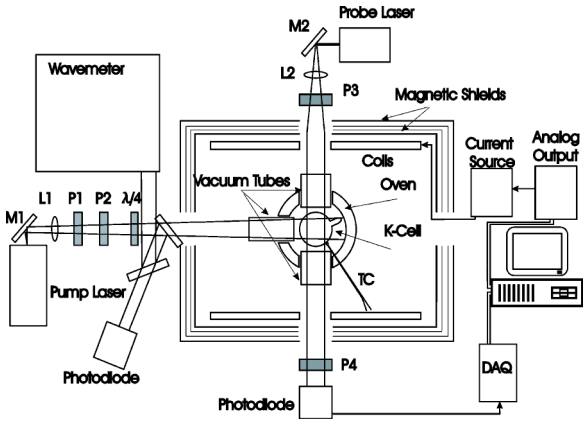

FIG. 1. Experimental setup for measurements of the Zeeman resonances in low magnetic field. P denotes polarizers; L, lenses; M, mirrors; and TC is a nonmagnetic thermocouple.

In numerical simulations we obtain the density matrix as a function of time and then calculate the evolution of the average spin $\mathbf{S}=\mathrm{Tr}[\mathbf{S}\rho]$. By fitting it with an exponentially decaying oscillation we obtain the decay constant T_2 and the resonance frequency ν_0 for comparison with experiment. In addition, we verified that the SE term conserves the total angular momenta, Eq. (4), and produces the spin-temperature distribution. Furthermore, we checked the simple qualitative picture of the spin-exchange phenomenon discussed in the previous section, i.e., that $\mathbf{F}_1$ and $\mathbf{F}_2$ precess in opposite directions when spin exchange is slow and precess together when spin exchange is fast.

IV. EXPERIMENT

A. Experimental setup

The experimental setup we have used in studies of magnetic resonances is shown in Fig. 1. The principle of operation is similar to that of the ultra-sensitive magnetometer described in Ref. [11]. The spin polarization is achieved via optical pumping with circularly polarized light, produced by a 500 mW master oscillator-power amplifier system. Two polarizers are added to the basic setup to control the intensity in a continuous fashion as the polarizer P1 is rotated. The incident intensity of the pump beam is measured with a photodiode, while the wavelength is monitored with a scanning Michelson interferometer wavemeter.

The transverse spin polarization is measured using optical rotation of a probe beam detuned off-resonance, generated by a broad area diode laser with a grating feedback. The optical rotation is measured by sending the probe beam through the polarizer P3, the potassium cell, and the second polarizer P4 which is rotated by 10° away from extinction. Both the pump and the probe lasers are expanded to illuminate the whole cell.

We use a 1 in. spherical aluminosilicate glass cell containing 12.5 atm of ^{4}He, 60 torr of N_2, and K metal in natural abundance. High buffer gas pressure ensures that the cell is optically thin even at high K density and reduces the light shift produced by the pump laser if it is slightly detuned from

resonance. The cell is placed inside a double-wall glass oven in which hot air flows between the walls, but does not cross the paths of the probe and pump beams which pass through evacuated glass tubes. The oven is well insulated to reduce heat losses and heating of the inner magnetic shield. The magnetic shield consists of 6 concentric hollow μ-metal cylinders with caps providing a 10^6 reduction of external fields. Magnetic fields inside the shields are created by a set of coils driven by a precision current source.

The probe beam intensity after the analyzer was measured by a photodiode and recorded by computer after amplification. The data were collected by applying a small oscillating B_y field and measuring the resulting signal using a lock-in amplifier implemented in a LabView program. The frequency of the B_y excitation was stepped across the magnetic resonance. The amplitude of the response was fit to the following function

$$\frac{h}{\sqrt{(\nu-\nu_0)^2+\Delta\nu^2}}+b+c\nu \tag{18}$$

to determine the magnetic resonance frequency ν_0 and the resonance HWHM $\Delta\nu=1/2\pi T_2$.

B. Relationship between theoretical and experimental parameters

For comparison of theory with experiment, we have to relate experimental parameters such as the temperature of the cell, current in the magnetic field coils, and the pump intensity to theoretical counterparts such as the SE rate, the magnetic field, and the polarization. The SE rate can be found from the density of the alkali-metal vapor and the SE cross section. The SE cross section for K atoms has been measured in [2,18] with values of $(1.45\pm0.2)\times10^{-14}$ cm^2 and $(1.8\pm0.1)\times10^{-14}$ cm^2, respectively. The density of the K vapor can be determined from the temperature of the cell if one assumes that the K vapor is saturated. The data for saturated K densities are given in reference books [19,20], at 170 °C they give 3.7×10^{13} cm^{-3} and 3.0×10^{13} cm^{-3}, respectively. The SE rate estimated by this method is equal to $A_{SE}=(3.7\pm0.7)\times10^4$ s^{-1}. Given a significant uncertainty in this estimate, we determine the SE rate directly from the data by fitting the variation of the gyromagnetic ratio as a function of the magnetic field at the lowest polarization (see Fig. 6), which gives $A_{SE}=(4.3\pm0.2)\times10^4$ s^{-1}. For a small fraction of the data that were not collected at 170 °C we assume that the K density changes with temperature in accordance with the slope given in [19].

The magnetic field along the z direction is created by a solenoid inside the magnetic shields. There is some concern that the saturation and hysteresis of the magnetic shields could lead to a nonlinear dependence of the magnetic field on the current in the coils. We verified using a flux-gate magnetometer that the magnetic field scales linearly with the current over the range of the magnetic fields studied and does not depend on the history of the applied current. There is a small magnetic field offset that remains stable over the course of the measurements and can be corrected in the calibration of the magnetic fields.

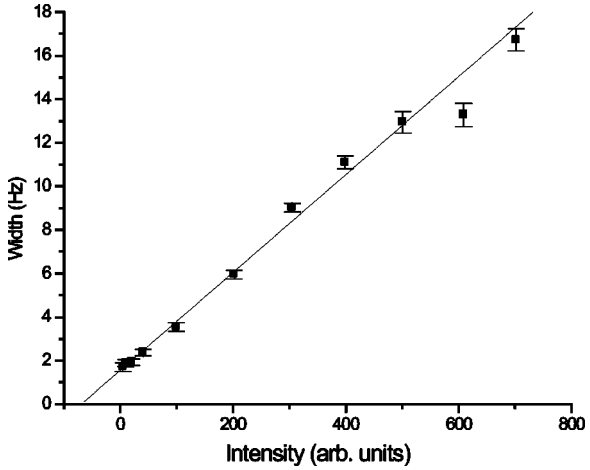

FIG. 2. Measurement of the Zeeman resonance half-width $\Delta\nu$ as a function of incident intensity of the pump beam.

The steady-state spin polarization P can be determined from Eq. (14). Neglecting the effects of diffusion which are small in a high buffer gas pressure cell, the equilibrium polarization is given by [17]

$$P=s\frac{R}{R+A_{SD}}. \tag{19}$$

It was shown in [11] that in the limit of low magnetic field and high alkali-metal density the resonance linewidth is given by $\Delta\nu=(R+A_{SD})/2\pi q$, where $q=1+I(I+1)/S(S+1)$ is the slowing down factor equal to 6 for $I=3/2$. The transverse relaxation found from fitting of the magnetic resonance width can, in principle, be different from the longitudinal relaxation rate, which determines the equilibrium polarization. However, by solving density matrix equations [Eq. (14)], it can be shown that they are equal when $\omega_0 T_{SE}\ll1$. In Fig. 2 we plot the width $\Delta\nu$ as a function of the pump intensity. The Zeeman resonance frequency for this data was 25 Hz, much smaller than the SE rate. The width is proportional to the intensity of the pump beam, which is expected for an optically thin alkali-metal vapor. The intercept of the line gives the spin-destruction rate $A_{SD}=59\pm5$ sec^{-1} and the slope gives the pumping rate R in terms of the incident intensity. The spin-destruction rate can also be calculated from the measured spin-destruction cross sections and the buffer gas composition [11], which gives $A_{SD}=49$ sec^{-1}, in good agreement with the measured value given uncertainties in the cross sections.

The degree of circular polarization s of the pump beam inside the cell is difficult to determine accurately. We expect it to be close to unity but birefringence of the cell walls or reflections of the pump beam inside the cell can reduce the degree of circular polarization. To remove this uncertainty we fit the measurements of the gyromagnetic ratio as a function of the polarization at low magnetic field to Eq. (10). We also found that a better measurement of A_{SD} can be obtained by expressing the polarization as $P=s(\Delta\nu-A_{SD}/2\pi q)/\Delta\nu$ and allowing s and A_{SD} to vary. Figure 3 shows a plot of the gyromagnetic ratio γ vs the resonance linewidth $\Delta\nu$. From

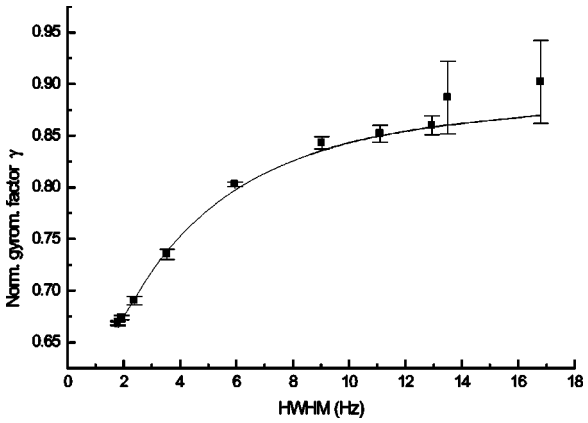

FIG. 3. The dimensionless gyromagnetic ratio γ as a function of the resonance linewidth $\Delta\nu$ in the regime of low magnetic field. The fit is based on Eqs. (10) and (19).

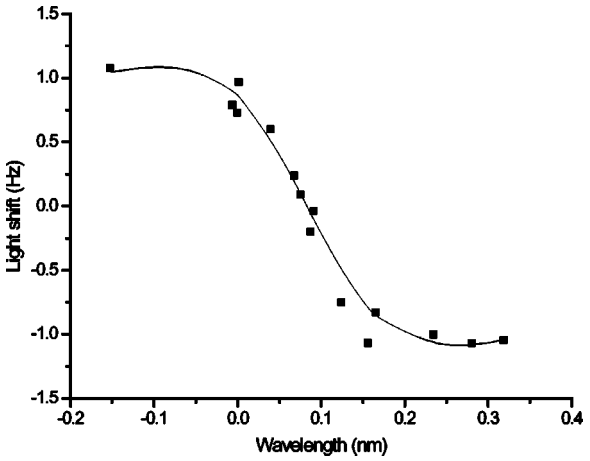

FIG. 4. The dependence of light shift caused by the pump laser on the wavelength near the 770 nm potassium D1 transition for 12.5 amg of He buffer gas.

the fit to the data we determine $s=0.82\pm0.01$ and $A_{SD}=63\pm1\ s^{-1}$. This determination of A_{SD} is consistent with the direct measurement of the linewidth at low pump power but has a smaller uncertainty.

A number of additional resonance broadening mechanisms have to be minimized to obtain reliable data. The broadening due to the optical pumping by the probe laser power and due to the excitation field B_y can be reduced by keeping both of them low, although at the expense of the signal strength. Nonuniform polarization of the atoms inside the cell leads to additional broadening because the gyromagnetic ratio depends on the polarization. Nonuniform distribution of the pump light intensity, relaxation by diffusion to cell walls, and pump beam distortions due to sphericity of the cell all can give raise to polarization nonuniformity. This type of broadening scales with the Zeeman frequency. Special care was taken to illuminate the cell with a uniform intensity pump beam and to minimize the optical depth. Based on simulations of possible polarization distributions we estimate that gyromagnetic ratio variation broadens the linewidth by no more than 10%. The light shift can also potentially broaden the resonance if the wavelength of the pump beam is not tuned to the center of the optical resonance and if the intensity distribution is not uniform. As discussed in more detail below, the light shift does not exceed 1 Hz because the pump laser was tuned to the center of the optical resonance. At low frequencies when $\Delta\nu$ is comparable to ν_0 the shape of the signal is distorted by the resonance at $-\nu_0$ excited by the counter-rotating component of the magnetic field. We checked that the fit based on Eq. (18) adequately describes the shape of the signal even when $\nu_0=30$ Hz and $\Delta\nu=20$ Hz.

C. Light shift

The potential systematic effect due to the light shift produced by the pump laser is particularly significant because we measure the magnetic resonance frequency as a function of the pump intensity. It is well known that the effect of the ac Stark shifts can be described by an equivalent magnetic field parallel to the direction of the laser and proportional its degree of circular polarization [21]. The light shift is proportional to the pumping rate and has a dispersion shape as a function of the wavelength of the laser, vanishing at the center of the resonance. For small detuning away from the D1 resonance in K the light shift is given by

$$\delta\nu_{LS}=\frac{R}{2\pi q}\frac{\lambda-\lambda_0}{\Delta\lambda}, \tag{20}$$

where $\lambda-\lambda_0$ is the detuning from the optical resonance and $\Delta\lambda$ is the HWHM determined by pressure broadening. Figure 4 shows a measurement of the light shift as a function of wavelength near 770 nm. It is described well by a dispersion profile with a HWHM=0.17 nm, consistent with measurements of pressure broadening of K by He buffer gas [22] which give HWHM=0.16 nm for 12.5 atm of He buffer gas. The wavelength of the pump laser was tuned to the point of vanishing light shift and maintained within 0.01 nm, ensuring that the light shift was less than 6% of the resonance linewidth.

D. rf broadening

The effects of rf broadening of magnetic resonance transitions are well understood and can be described by Bloch equations. The magnetic resonance width in the presence of a strong oscillating B_y field is given by [14]

$$\Delta\nu_{RF}=\Delta\nu(1+\omega_y^2T_1T_2)^{1/2}, \tag{21}$$

where ω_y is the frequency of spin precession in the B_y field. In a dense alkali-metal vapor T_2 is often determined by spin-exchange collisions, while T_1 is determined by the optical pumping and spin-relaxation rate. As was first discovered in [13], increasing the pumping rate can reduce T_1 without significantly affecting T_2 and lead to narrowing of the magnetic resonance. In our experiment we observed that at low pump intensity the effect of rf broadening was the strongest. For example, at a pumping rate of 40 sec^{-1} when the rf amplitude was increased from 7.4 μG to 120 μG, the resonance broadened from 2.6 Hz to 8 Hz. At a higher pumping rate of

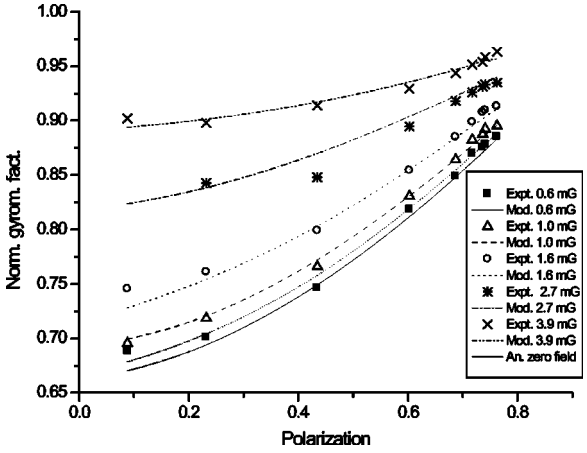

FIG. 5. The dependence of the normalized gyromagnetic factor $\gamma=\omega/\omega_0$ on the polarization for several values of the magnetic field. Agreement between numerical simulations and experiment is close except for a few points of large polarization. The analytical result at zero field Eq. (10) completely agrees with numerical simulations. In order to distinguish them we did not plot the numerical solution at zero field.

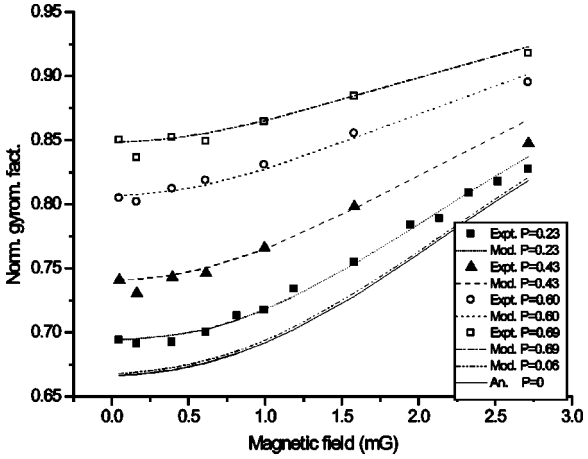

FIG. 6. The dependence of the normalized gyromagnetic factor $\gamma=\omega/\omega_0$ on the magnetic field for several values of the polarization. The experimental points, shown by various symbols, follow curves predicted in the numerical simulation. In the case of zero polarization, the simulation also agrees with the analytical result Eq. (23).

120 sec^{-1} the linewidth increased only from 4.8 Hz to 6.2 Hz for the same change in the rf amplitude. By analyzing these experimental data we were able to find the optimal amplitude of the rf field which gives an acceptable signal-to-noise ratio and does not cause significant broadening and frequency shift.

E. Measurements of magnetic resonances and comparison with simulations

1. Gyromagnetic factor

The first important test of theory and our experimental technique is to measure the resonance frequency at low magnetic fields in the regime of fast spin exchange. According to Eq. (9) the frequency should change from $(2/3)\omega_0$ to ω_0 when the pump intensity increases from very small to very large values. Although very small values are limited by sensitivity and very large values are limited by the maximum available power, we could cover a range of about 100 in intensity and obtain the ratio of maximum to minimum frequency close to 1.5 expected from theory. The residual deviation from theory can be attributed to imperfections of circular polarization and nonuniformity of pump intensity. We found experimentally that by reducing the pump beam size we could broaden the resonance and make the experimental data deviate from a single Lorentzian profile.

Apart from the range comparison $\gamma(I_{\max})/\gamma(I_{\min})$, we also made a comparison of the gyromagnetic factors with theory for intermediate values of the polarization. The comparison for low and intermediate magnetic field data is shown in Fig. 5. The measurements at the lowest magnetic field follow well the analytical curve given by Eq. (10). A fit to these data is used to determined the values of s and A_{SD} that are used in the rest of the analysis (see Fig. 3).

The data in Fig. 5 at higher magnetic fields illustrate (i) the deviation of the experiment from Eq. (10) and (ii) the agreement with density matrix simulations. We found that numerical data for $\omega_0 T_{SE}<0.3$ can be interpolated with a simple equation

$$\gamma = 2 - \frac{4}{3 + 2.816(\omega_0 T)^2 + [1 - 2.544(\omega_0 T)^2]P^2}, \quad (22)$$

which is similar to Eq. (10). In Fig. 6 we plot the gyromagnetic factor as a function of magnetic field for several values of the polarization. The measurements at the lowest polarization ($P=0.23$) were used to determine the SE rate. Our experimental data agree well with the numerical simulation for all values of the polarization. The low polarization case was investigated experimentally by Happer and Tang [5] in Cs and theoretically by Happer and Tam [6] who derived an analytical equation valid for arbitrary SE rate and low polarization. For potassium, $I=3/2$, this equation can be rewritten as

$$\frac{\kappa}{\omega_0} = -\frac{3}{8\omega_0 T_{SE}} + \sqrt{-1 + \frac{i}{2\omega_0 T_{SE}} + \left[\frac{3}{8\omega_0 T_{SE}}\right]^2}, \quad (23)$$

where the real and imaginary parts of κ give the resonance width and the frequency, $\kappa=-2\pi(\Delta\nu+i\nu)$. Figure 6 illustrates close agreement of this equation with our numerical simulations for low polarization, $P=0.06$. At higher polarization, the gyromagnetic factor becomes less dependent on the magnetic field which can be explained by the fact that only the stretched state with the maximum m_F becomes populated and SE collisions become less important.

2. Width

The comparison of experiment and theory for widths of magnetic resonances is shown for low field, fast SE regime in Fig. 7 and for a large range of magnetic fields, slow and

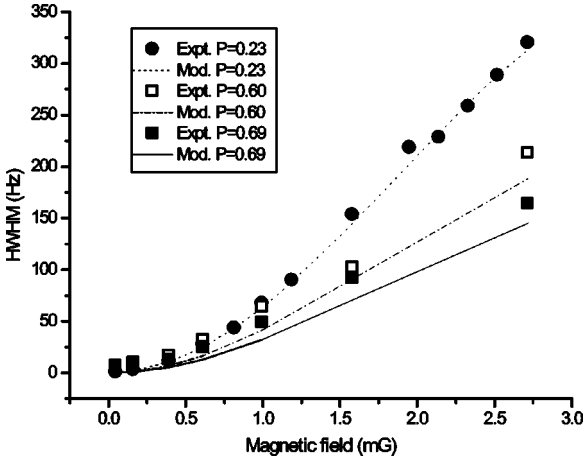

FIG. 7. The dependence of the width $\Delta\nu$ on the magnetic field for different values of the polarization.

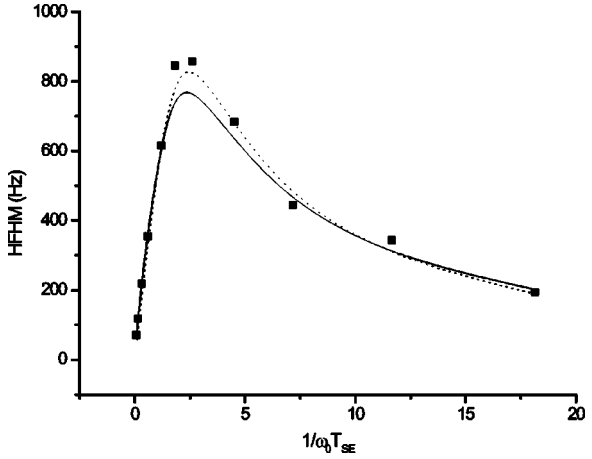

FIG. 8. The comparison of measured linewidth with values obtained from numerical simulations and from Eq. (23) for a full range of SE rates. In the experiment we varied both the temperature of the cell and the magnetic field and the data were rescaled to $B_z = 6.67$ mG and to temperature of 170 °C. The polarization of the vapor was kept low, on the order of 10%.

fast spin exchange, in Fig. 8. We find a particularly close agreement of experimental data with simulations for low polarization. In the case of larger polarization, the resonance has additional broadening due to the variation of the gyromagnetic ratio. Note that at large magnetic field the width decreases for larger polarization corresponding to larger pump intensity. Similar light narrowing was observed previously by Appelt *et al.* [15]. Compared to their study, in our case the individual Zeeman resonances are not resolved, but the overall behavior is very similar.

It is interesting to investigate the resonance width for a larger range of SE rates (Fig. 8). At small values of $1/\omega_0 T_{SE}$, the experimental width is proportional to SE rate $1/T_{SE}$, while at large $1/\omega_0 T_{SE}$, the width is proportional to T_{SE} in good agreement with Eq. (23). Numerical simulations are also in good agreement with experiment and analytical expressions. Near the maximum of the width, some disagreement is observed since a single exponential is not an accurate approximation of the polarization decay.

V. CONCLUSION

In this paper, we have investigated experimentally and theoretically the effects of spin-exchange collisions on the magnetic resonances for arbitrary magnetic field, polarization, and spin-exchange rates. The theory, based on the numerical solution of the density matrix equations, and the experiment agree well. We also verified numerically and experimentally analytical results in the limit of low magnetic field and in the limit of low polarization. A simple qualitative picture of the behavior of spins is also developed. This study of spin exchange will be useful for ultrasensitive magnetometers that operate at a nonzero magnetic field, at moderate density of alkali-metal atoms or at high frequency, that is in the regime when the precession frequency is comparable to the spin-exchange rate. The results of this work can also be used to determine the properties of the alkali-metal vapor, such as its density and polarization, from measurements of magnetic resonances in a low magnetic field and at high alkali-metal density.

Although we performed simulations and measurements for potassium, the results for other alkali-metal atoms are expected to be similar. The spin-exchange cross sections are nearly the same for all alkali metals and the only difference is in the value of the nuclear spin I. The dependence of the gyromagnetic ratio on the polarization in the limit of low field is given analytically for $I=3/2$, $5/2$, and $7/2$ in Eqs. (10)–(12), while general results for the gyromagnetic ratio and linewidth in the limit of low polarization are given in [6]. For higher nuclear spins the gyromagnetic ratio changes by a larger factor as a function of the polarization, for example for Cs ($I=7/2$) it changes by a factor of $11/4$. In the case of Rb in natural abundance, the effects of spin-exchange between the two isotopes with $I=3/2$ and $I=5/2$ will lead to additional broadening and changes in the gyromagnetic ratio, but the broadening due to the SE collisions and the differences in the gyromagnetic ratio still vanish as B^2 in the limit of low fields. The spin-destruction cross sections are larger for heavier alkali atoms, so the magnetic resonance linewidth would be broader even in the absence of SE, which makes heavier alkali metals less favorable candidates for magnetometers.

ACKNOWLEDGMENTS

We would like to thank Adrian Liu and David Hsieh for construction of parts of the apparatus. This work was supported by the NSF, Packard Foundation, and Princeton University.

[1] J. P. Wittke and R. H. Dicke, Phys. Rev. **103**, 620 (1956).
[2] N. W. Ressler, R. H. Sands, and T. E. Stark, Phys. Rev. **184**, 102 (1969).
[3] H. M. Gibbs and R. J. Hull, Phys. Rev. **153**, 132 (1967).
[4] H. W. Moos and R. H. Sands, Phys. Rev. **135**, A591 (1964).
[5] W. Happer and H. Tang, Phys. Rev. Lett. **31**, 273 (1973).
[6] W. Happer and A. C. Tam, Phys. Rev. A **16**, 1877 (1977).
[7] F. Grossetête, J. Phys. (Paris) **25**, 383 (1965).
[8] H. Gibbs, Phys. Rev. **139**, A1374 (1965).
[9] L. W. Anderson, F. M. Pipkin, and J. C. Baird, Phys. Rev. **116**, 87 (1959).
[10] L. W. Anderson and A. T. Ramsey, Phys. Rev. **132**, 712 (1963).
[11] J. C. Allred, R. N. Lyman, T. W. Kornack, and M. V. Romalis, Phys. Rev. Lett. **89**, 130801 (2002).
[12] I. K. Kominis, T. W. Kornack, J. C. Allred, and M. V. Romalis, Nature (London) **422**, 596 (2003).
[13] N. D. Bhaskar, J. Camparo, W. Happer, and A. Sharma, Phys. Rev. A **23**, 3048 (1981).
[14] A. Abragam, *Principles of Nuclear Magnetism* (Oxford University Press, New York, 1961).
[15] S. Appelt, A. B.-A. Baranga, A. R. Young, and W. Happer, Phys. Rev. A **59**, 2078 (1999).
[16] Y. Jau, A. Post, N. Kuzma, A. Braun, M. Romalis, and W. Happer, Phys. Rev. Lett. **92**, 110801 (2004).
[17] S. Appelt, A. B.-A. Baranga, C. J. Erickson, M. V. Romalis, A. R. Young, and W. Happer, Phys. Rev. A **58**, 1412 (1998).
[18] E. Aleksandrov, M. Balabas, A. Vershovskii, A. Okunevich, and N. Yakobson, Opt. Spectrosc. **87**, 329 (1999); **93**, 488(E) (2002).
[19] *Handbook of Physical Quantities*, edited by I. S. Grigoriev and E. Z. Meilikhov (CRC Press, New York, 1997).
[20] *Handbook of Chemistry and Physics*, 78th ed., edited by D. R. Lide (CRC Press, New York, 1997–1998).
[21] W. Happer and B. S. Mathur, Phys. Rev. **163**, 12 (1967).
[22] N. Lwin and D. G. McCartan, J. Phys. B **11**, 3841 (1978).